Acta Materialia 207 (2021) 116665

Contents lists available at ScienceDirect

Acta Materialia

journal homepage: www.elsevier.com/locate/actamat

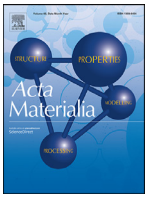

Influence of Ni_4Ti_3 precipitation on martensitic transformations in NiTi shape memory alloy: R phase transformation

Jiaming Zhu[a,b,*], Hong-Hui Wu[c], Yuan Wu[c], Haoliang Wang[d], Tianlong Zhang[f], Hu Xiao[g], Yunzhi Wang[e,*], San-Qiang Shi[b,*]

[a] *School of Civil Engineering, Shandong University, Jinan 250061, China*
[b] *Department of Mechanical Engineering, The Hong Kong Polytechnic University, Hong Kong, China*
[c] *State Key Laboratory for Advanced Metals and Materials, University of Science and Technology Beijing, Beijing 100083, China*
[d] *Department of Mechanical Engineering, Dongguan University of Technology, China*
[e] *Department of Materials Science and Engineering, The Ohio State University, 2041 College Road, Columbus, OH 43210, USA*
[f] *Department of Materials Science and Engineering, City University of Hong Kong, Tat Chee Avenue, Kowloon Tong, Kowloon, Hong Kong, China*
[g] *Center of Microstructure Science, Frontier Institute of Science and Technology, Xi'an Jiaotong University, Xi'an 710049, China*

ARTICLE INFO

Article history:
Received 22 September 2020
Revised 15 December 2020
Accepted 16 January 2021
Available online 20 January 2021

Keywords:
Martensitic transformation
Ni_4Ti_3 precipitates
Shape memory alloy
R phase transformation
Phase field method

ABSTRACT

Precipitation of Ni_4Ti_3 is effective in tuning martensitic transformations (MTs) in NiTi shape memory alloys (SMAs). However, several fundamental issues concerning the influence of Ni_4Ti_3 on MTs remain unclear. In this study, the microstructure evolution process during precipitation and its influence on B2→R MT are investigated using computer simulations based on the phase field method. In particular, the roles played by Ni concentration gradient in the B2 matrix and internal coherency stress fields associated with different precipitate microstructures are analyzed in detail. It is found that Ni concentration gradient in the B2 matrix created by Ni_4Ti_3 precipitates alters significantly local martensitic start temperature and the overall MT behavior, while the internal coherency stress field associated with the Ni_4Ti_3 precipitates dictates the structure of martensitic domains via variant selection. The latter effect makes it promising to develop Invar alloys via stress-ageing to tailor the precipitate microstructure. These findings provide fundamental insights into the mechanism controlling the MT behavior in precipitate-bearing SMAs and provide guidance for the design of thermomechanical treatment for desired precipitate microstructures and the corresponding MT behavior.

1. Introduction

NiTi shape memory alloys (SMAs) have many attractive applications in functional devices such as actuators, sensors, vascular stents, active medical catheters, to name a few [1–3], because of their unique shape memory effect and super-elasticity. The characteristics of martensitic transformations (MTs) in SMAs control the performance of SMA devices. Recent studies have demonstrated that nanoscale concentration modulation [4–7] and internal stress fields induced by point defects [8,9], dislocations [10,11] and nanovoids [12,13] can alter drastically the characteristics of MTs, making a typical sharp first-order transition into a continuous transformation. In fact, nanoprecipitates have been utilized in SMAs to tailor MTs long time ago. These precipitates create concentration heterogeneity, coherency stress field and geometrical confinement in the parent phase, all of which will impact significantly the characteristics of MTs. In Ni-rich NiTi SMAs, for example, introducing Ni_4Ti_3 precipitates is a simple and low-cost way to tune the characteristics of MTs, including the MT types, the MT start temperature, and the first-order or continuous nature of the MT. It has been well documented that the appearance of Ni_4Ti_3 precipitates changes the properties of NiTi SMAs drastically by converting the transformation path from the otherwise single-stage B2→B19′ MT to a two-stage B2→R→B19′ MT [14,15], and that the start temperatures of R phase transformation (R_s) and B19′ phase transformation (M_s) can be tuned by controlling the ageing temperature [16]. More complicated MT behaviors have also been reported [17–22], including complicated MT sequences of one B2→R transformation followed by two R→B19′ transformations [23,24], and one B2→R transformation followed by a B2→ B19′ transformation and a R→B19′ transformation [25] observed in Ni51.14 at.%-Ti, Ni51.3 at.%-Ti, and Ni50.6 at.%-Ti alloys aged at 673-823 K. When aged at lower temperatures, e.g. 473-573 K [26], the MT sequence

---

* Corresponding author.
E-mail addresses: zhujiaming@sdu.edu.cn (J. Zhu), wang.363@osu.edu (Y. Wang), san.qiang.shi@polyu.edu.hk (S.-Q. Shi).

https://doi.org/10.1016/j.actamat.2021.116665

in the alloy changed to two B2→R MTs followed by one R→ B19′ MT.

In order to understand how a precipitate microstructure in the parent phase influences the MT behavior, one needs to investigate MT process in different local precipitate environment. This could be a daunting task for experiments because ageing treatment usually generates complicated precipitate microstructures. Also, it is challenging to experimentally differentiate the contributions from internal stress and from concentration heterogeneity to the driving force for MTs. In contrast, it is convenient to achieve these goals by computer simulations using the phase field method [27–36]. In this study we carry out a systematic study on the influence of Ni_4Ti_3 precipitates on MTs in NiTi SMAs using the phase field method. In contrast to the previous study [30], phase field models of both Ni_4Ti_3 precipitate and R phase transformation are developed, and the MT processes in systems having different initial compositions and being aged for different times, containing both single and multiple Ni_4Ti_3 particles are investigated. It is well known that, in solution treated NiTi SMA alloys, the B2 phase directly transforms into the B19′ phase upon cooling, while in precipitate-bearing NiTi SMA alloys, the B2 phase first transforms into R phase and then to B19′ phase. The reason behind this is believed to be that precipitates act as a much stronger obstacle to the B2 to B19′ transformation than that to the B2 to R transformation because the former has a much larger transformation strain [14]. To limit the scope of this study, we confine our interest to the R phase transformation. Below, we first present phase field models for Ni_4Ti_3 precipitates (Section 2.1) and R phase transformation (Section 2.2) based on Landau theory [37], gradient thermodynamics [38,39], and the Khachaturyan–Shatalov's microelasticity theory [40] of structural phase transformations. The evolution of Ni_4Ti_3 precipitate microstructure with ageing time in different alloys is studied in Section 3, together with its influence on the R phase transformation. The contribution of concentration heterogeneity and internal stress (i.e., coherency stress) field in the B2 matrix phase caused by Ni_4Ti_3 precipitation, and the geometrical constraint created by the precipitates to the R phase transformation are discussed in Section 4. Finally, the main findings are summarized in Section 5.

2. Development of phase field models

The microstructure formed by Ni_4Ti_3 precipitates is a function of ageing temperature and initial composition. Moreover, the relative thermodynamic stability between the parent and R phase is composition-dependent. All of these facts are considered in this study as presented below, in contrast to previous models.

2.1. Phase field model of precipitation of Ni_4Ti_3

2.1.1. Gibbs free energy of B2 matrix and Ni_4Ti_3 precipitate

The parent phase, i.e. the matrix, of NiTi SMA alloy has a B2 lattice structure. It is reported that, in NiTi alloys, the largest site fraction of vacancies is merely in the order of 10^{-3} even at 1200 K [41]. Therefore, the influence of vacancies on Gibbs free energy of NiTi alloys can be safely neglected. Following literature [42], the $(Ni, Ti)_{0.5}(Ni, Ti)_{0.5}$ sublattice model is adopted and the Gibbs free energy of the B2 matrix is formulated as

$$\begin{aligned} G_{B2} = {} & y^{I}_{Ni} y^{II}_{Ti} G_{Ni:Ti} + y^{I}_{Ti} y^{II}_{Ni} G_{Ti:Ni} \\ & + \frac{RT}{2}\left(y^{I}_{Ni}\ln y^{I}_{Ni} + y^{I}_{Ti}\ln y^{I}_{Ti} + y^{II}_{Ni}\ln y^{II}_{Ni} + y^{II}_{Ti}\ln y^{II}_{Ti}\right) \\ & + y^{I}_{Ni} y^{I}_{Ti} \sum_{j}\left(y^{II}_{Ni} L^{j}_{Ni,Ti:Ni} + y^{II}_{Ti} L^{j}_{Ni,Ti:Ti}\right)\left(y^{I}_{Ni} - y^{I}_{Ti}\right)^{j} \\ & + y^{II}_{Ni} y^{II}_{Ti} \sum_{j}\left(y^{I}_{Ni} L^{j}_{Ni:Ni,Ti} + y^{I}_{Ti} L^{j}_{Ti:Ni,Ti}\right)\left(y^{II}_{Ni} - y^{II}_{Ti}\right)^{j} \end{aligned} \tag{1}$$

Table 1
Lattice correspondence between B2 phase and Ni_4Ti_3 variants [44].

Variant No.	$[100]_{Ni_4Ti_3}$	$[010]_{Ni_4Ti_3}$	$[001]_{Ni_4Ti_3}$
1	$[\bar{4}5\bar{1}]_{B2}$	$[\bar{2}\bar{1}3]_{B2}$	$[111]_{B2}$
2	$[\bar{5}41]_{B2}$	$[12\bar{3}]_{B2}$	$[\bar{1}\bar{1}\bar{1}]_{B2}$
3	$[\bar{4}\bar{5}1]_{B2}$	$[\bar{2}1\bar{3}]_{B2}$	$[1\bar{1}\bar{1}]_{B2}$
4	$[\bar{5}\bar{4}\bar{1}]_{B2}$	$[1\bar{2}3]_{B2}$	$[\bar{1}11]_{B2}$
5	$[451]_{B2}$	$[2\bar{1}\bar{3}]_{B2}$	$[\bar{1}1\bar{1}]_{B2}$
6	$[54\bar{1}]_{B2}$	$[\bar{1}23]_{B2}$	$[1\bar{1}1]_{B2}$
7	$[4\bar{5}\bar{1}]_{B2}$	$[213]_{B2}$	$[\bar{1}\bar{1}1]_{B2}$
8	$[5\bar{4}1]_{B2}$	$[\bar{1}\bar{2}\bar{3}]_{B2}$	$[11\bar{1}]_{B2}$

$$0.5y^{I}_{Ni} + 0.5y^{II}_{Ni} = c_{Ni} \tag{2a}$$

$$0.5y^{I}_{Ti} + 0.5y^{II}_{Ti} = c_{Ti} \tag{2b}$$

$$y^{I}_{Ni} + y^{I}_{Ti} = 1 \tag{2c}$$

$$y^{II}_{Ni} + y^{II}_{Ti} = 1 \tag{2d}$$

where y^{I}_{i} and y^{II}_{i} denote the site fraction of i on sublattice I and II, respectively. At any given temperature and composition, the phases must be at internal equilibrium determined by $\frac{\partial G_{B2}}{\partial y} = 0$ for all site fractions ($y = y^{I}_{Ni},\ y^{I}_{Ti},\ y^{II}_{Ni},$ or y^{II}_{Ti}).

Since Ni_4Ti_3 is a stoichiometric phase with a small stability range, for simplicity, its Gibbs free energy of the Ni_4Ti_3 phase is estimates via [30,43]

$$\begin{aligned} G_{Ni_4Ti_3} = {} & A_1c^2 + A_2c + A_3 + A_4T + A_5T\ln T + A_6T^2 + A_7T^3 + A_8T^{-1} \\ & + 3G^{hcp,0}_{Ti} + 4G^{fcc,0}_{Ni} - 4G^{bcc,0}_{Ni} - 3G^{bcc,0}_{Ti} \end{aligned} \tag{3}$$

All parameters used in Eqs. (1) and(3) are given in the Appendix.

2.1.2. Stress-free transformation strain of Ni_4Ti_3 precipitate

The parent phase possesses a B2 (cubic) lattice structure with a lattice parameters of $a_0 = 0.3015$ nm, and the Ni_4Ti_3 phase has a rhombohedral lattice structure with lattice parameters of $a_{Ni_4Ti_3} = 0.6704$ nm and $\alpha_{Ni_4Ti_3} = 113.83^\circ$ [30]. The symmetry breaking accompanying the lattice transformation from cubic to rhombohedral leads to 8 precipitate variants [44]. In the principal reference of variant 1 of Ni_4Ti_3 phase, the stress-free transformation strain (SFTS) of variant 1 can be written as [30]

$$\begin{bmatrix} -0.00417 & 0 & 0 \\ 0 & -0.00417 & 0 \\ 0 & 0 & -0.0257 \end{bmatrix} \tag{4}$$

The SFTS of the other variants are the same as Eq. (4) in their own principal references. In this study, we set the axes of a global reference parallel to the three cubic directions of the B2 phase. The SFTS of the 8 precipitate variants can be transformed from their local references to the global reference via the lattice correspondence listed in Table 1.

2.1.3. Total free energy of the precipitate-bearing system

In addition to Ni concentration, the parent B2 and precipitate Ni_4Ti_3 phases are also characterized by a set of non-conserved structural order parameters, $\phi = \{\phi_1, \ldots, \phi_8\}$, with $\phi_{p=1-8} = 0$ representing the parent phase and $\phi_p = 1,\ \phi_{q=1-8,\ \text{but}\ q\neq p} = 0$ representing the p-th variant of the Ni_4Ti_3 precipitate. The total free energy of the system is formulated as

$$F^{P} = \int \left(f^{P}_{ch} + f^{P}_{gr}\right) d^3\boldsymbol{r} + E^{P}_{el} \tag{5}$$

where f^{P}_{ch}, f^{P}_{gr} and E^{P}_{el} represent the chemical free energy density, the gradient energy density and the total elastic energy, respectively.

The chemical free energy density is formulated as

$$f_{\mathrm{ch}}^{\mathrm{P}}=\frac{1}{V_{\mathrm{m}}}\left\{h\left(\sum_{\mathrm{p}=1}^{8}\phi_{\mathrm{p}}\right)G_{\mathrm{Ni_4Ti_3}}+\left[1-h\left(\sum_{\mathrm{p}=1}^{8}\phi_{\mathrm{p}}\right)\right]G_{\mathrm{B2}}+\Psi_1\sum_{\mathrm{p}=1}^{8}|\phi_{\mathrm{p}}||1-\phi_{\mathrm{p}}|+\Psi_2\sum_{\mathrm{p}=1}^{8}\sum_{\mathrm{q}>\mathrm{p}}^{8}\phi_{\mathrm{p}}^2\phi_{\mathrm{q}}^2\right\} \tag{6}$$

where $V_{\mathrm{m}}=1\times10^{-5}$ m^{3}mol^{-1} [30] denotes molar volume of NiTi alloy, $h(\phi)=\phi^3(10-15\phi+6\phi^2)$ is an interpolation function connecting the free energies of the B2 and $\mathrm{Ni_4Ti_3}$ phases, which satisfies the constrains that $h(0)=0$, $h(1)=1$ and $\mathrm{d}h/d\phi=0$ at $\phi=0$ and 1 to make thermodynamic equilibrium values of ϕ remain at 0 and 1 [45]. $\Psi_1=5\times10^5$ Jm^{-3} [46] characterizes the energy barrier between the parent phase and $\mathrm{Ni_4Ti_3}$ and $\Psi_2=2.9\times10^8$ Jm^{-3} [46] represents the energy barrier among different precipitate variants along the minimum energy path on the total chemical free energy landscape.

Following the gradient thermodynamics [38], the gradient energy density reads

$$f_{\mathrm{gr}}^{\mathrm{P}}=\frac{1}{2}\kappa_c\left(\nabla c_{\mathrm{Ni}}\right)^2+\frac{1}{2}\kappa_\phi\sum_{\mathrm{p}=1}^{8}\left(\nabla\phi_{\mathrm{p}}\right)^2 \tag{7}$$

where $\kappa_{\mathrm{c}}=6.9\times10^{-9}$ Jm^{-1} and $\kappa_\phi=7\times10^{-10}$ Jm^{-1} [30] are the gradient energy coefficients for chemical and structural non-uniformities, respectively.

The elastic energy is calculated via the Khachaturyan's microelasticity theory [40] which has the following close form

$$E_{\mathrm{el}}^{\mathrm{P}}=\frac{1}{2}\sum_{\mathrm{p}=1}^{8}\sum_{\mathrm{q}=1}^{8}\int\frac{d^3k}{(2\pi)^3}B_{\mathrm{pq}}(\boldsymbol{n})\left\{\phi_{\mathrm{p}}^2\right\}_k\left\{\phi_{\mathrm{q}}^2\right\}_k^* \tag{8}$$

where the integral is taken in the reciprocal space, $\boldsymbol{n}=\frac{\boldsymbol{k}}{k}$ is a unit vector and $\boldsymbol{k}$ is a vector with modulus k in the reciprocal space (note that $\boldsymbol{k}=0$ is to be excluded from the integration), $\{\phi_{\mathrm{p}}^2\}_k$ is the Fourier transformation of ϕ_{p}^2, and $\{\phi_{\mathrm{q}}^2\}_k^*$ represents the complex conjugate of $\{\phi_{\mathrm{q}}^2\}_k$. For a system with a fix boundary, $B_{\mathrm{pq}}(\boldsymbol{n})$ in Eq. (8) reads

$$B_{\mathrm{pq}}(\mathbf{n})=\begin{cases}C_{\mathrm{ijkl}}\varepsilon_{\mathrm{ij}}^{\mathrm{P}}(\mathrm{p})\varepsilon_{\mathrm{kl}}^{\mathrm{P}}(\mathrm{q}) & n=0\\ C_{\mathrm{ijkl}}\varepsilon_{\mathrm{ij}}^{\mathrm{P}}(\mathrm{p})\varepsilon_{\mathrm{kl}}^{\mathrm{P}}(\mathrm{q})-n_{\mathrm{i}}\sigma_{\mathrm{ij}}^{0}(\mathrm{p})\Omega_{\mathrm{jk}}(\mathbf{n})\sigma_{\mathrm{kl}}^{0}(\mathrm{q})n_{\mathrm{l}} & n\neq0\end{cases} \tag{9}$$

where $\varepsilon_{\mathrm{ij}}^{\mathrm{P}}(\mathrm{p})$ denotes the SFTS of the p-th $\mathrm{Ni_4Ti_3}$ variant, $\sigma_{\mathrm{ij}}^{0}(\mathrm{p})=C_{\mathrm{ijkl}}\varepsilon_{\mathrm{kl}}^{\mathrm{P}}(\mathrm{p})$, $\Omega_{\mathrm{ij}}^{-1}(\boldsymbol{n})=C_{\mathrm{iklj}}n_{\mathrm{k}}n_{\mathrm{l}}$. The elastic constants of NiTi alloy are C_{11}=183 GPa, C_{12}=146 GPa and C_{44}=46 GPa [47].

2.1.4. Kinetic equation

The temporal and spatial evolution of concentration and structural order parameters is described by Cahn-Hilliard [48] and Ginzberg-Landau [49] equation, respectively.

$$\frac{1}{V_{\mathrm{m}}^2}\frac{\partial c_{\mathrm{Ni}}}{\partial t}=\nabla\cdot\left[M\nabla\left(\frac{\delta F^{\mathrm{P}}}{\delta c_{\mathrm{Ni}}}\right)\right] \tag{10}$$

$$\frac{\partial\phi_{\mathrm{p}}}{\partial t}=-L_\phi\frac{\delta F^{\mathrm{P}}}{\delta\phi_{\mathrm{p}}},\ \ \mathrm{p}=1-\ 8 \tag{11}$$

where $M=\frac{D}{V_{\mathrm{m}}^2\frac{\partial^2 f_{\mathrm{ch}}^{\mathrm{P}}}{\partial c_{\mathrm{Ni}}^2}}$ is chemical mobility, $D=4.7\times10^{-9}\exp(\frac{-1.428\times10^5}{RT})$ m^{2}s^{-1} [50] is interdiffusion coefficient, R is the gas constant, and $L_\phi=0.882\times10^{-10}$ m^{3}J^{-1}s^{-1} [30] is the kinetic coefficient for structural evolutions.

2.2. Phase field model of B2→R martensitic transformation

2.2.1. Stress-free transformation strain of R phase

The trigonal R phase has 4 crystallographic equivalent variants [51]. The transformation matrices that map the parent phase lattice onto that of the R phase variants by a uniform lattice distortion read [14]

$$\mathbf{U}_1=\begin{bmatrix}\rho&\gamma&\gamma\\\gamma&\rho&\gamma\\\gamma&\gamma&\rho\end{bmatrix},\mathbf{U}_2=\begin{bmatrix}\rho&\gamma&-\gamma\\\gamma&\rho&-\gamma\\-\gamma&-\gamma&\rho\end{bmatrix},\mathbf{U}_3=\begin{bmatrix}\rho&-\gamma&\gamma\\-\gamma&\rho&-\gamma\\\gamma&-\gamma&\rho\end{bmatrix},\mathbf{U}_4=\begin{bmatrix}\rho&-\gamma&-\gamma\\-\gamma&\rho&\gamma\\-\gamma&\gamma&\rho\end{bmatrix} \tag{12}$$

where $\rho=\frac{\sqrt{6}a_{\mathrm{R}}+\sqrt{3}c_{\mathrm{R}}}{9a_0}$, $\gamma=\frac{-\sqrt{6}a_{\mathrm{R}}+2\sqrt{3}c_{\mathrm{R}}}{18a_0}$, with $a_{\mathrm{R}}=0.7339$ nm, $c_{\mathrm{R}}=0.5284$ nm and $a_0=0.3015$ nm [14] being the lattice parameters of the R phase and the parent phase, respectively. Note that the variation of lattice parameter of parent phase with composition is not considered in this model because of its weak dependence on composition [52]. The corresponding SFTS of the p-th variant, $\boldsymbol{\varepsilon}^{\mathrm{R}}(\mathrm{p})$, can be calculated directly from the transformation matrices given in Eq. (12) according to the following equation

$$\boldsymbol{\varepsilon}^{\mathrm{R}}(\mathrm{p})=\frac{1}{2}\left(\boldsymbol{U}_{\mathrm{p}}^{\mathrm{T}}\boldsymbol{U}_{\mathrm{p}}-\boldsymbol{I}\right),\ \ (\mathrm{p}=1-4) \tag{13}$$

where the superscript T indicates matrix transpose, and $\boldsymbol{I}$ is the identity matrix.

2.2.2. Free energy formulation

The R martensitic phase is distinguished from the parent B2 phase by introducing a set of 4 non-conserved structural order parameters, η_{p} (p=1-4), with $(\eta_{\mathrm{p}=1-4}=0)$ representing the parent B2 phase and $(\eta_{\mathrm{p}}=\pm1,\ \eta_{\mathrm{q}=1-4,\ \mathrm{q}\neq\mathrm{p}}=0)$ representing the p-th correspondence variant of the martensitic phase. The free energy functional of the system is formulated as the following

$$F^R=\int\left[\frac{1}{2}\kappa_\eta\sum_{\mathrm{p}=1}^{4}\left(\nabla\eta_{\mathrm{p}}\right)^2+f_{\mathrm{ch}}^{\mathrm{R}}+f_{\mathrm{in}}^{\mathrm{R}}\right]d^3r+E_{\mathrm{el}}^{\mathrm{R}} \tag{14}$$

where $\kappa_\eta=1.5\times10^{-11}$ Jm^{-1} [53] is the gradient energy coefficient for structural non-uniformities following the gradient thermodynamics [38], $f_{\mathrm{ch}}^{\mathrm{R}}$ is the Landau free energy density that describes the free energy of a local unit volume element having a uniform structural state characterized by $\eta_{\mathrm{p}}(\boldsymbol{r})$ (p=1-4) [54–57], $f_{\mathrm{in}}^{\mathrm{R}}$ is the interaction free energy density characterizing the interaction between precipitate-induced coherent stress fields and R phase [12,58–60]. The Landau free energy density can be approximated by the following polynomial [27]

$$f_{\mathrm{ch}}^{\mathrm{R}}=\frac{1}{2}A_1^{\mathrm{R}}(T-T_0)\sum_{\mathrm{p}=1}^{4}\eta_{\mathrm{p}}^2-\frac{1}{4}A_2^{\mathrm{R}}\sum_{\mathrm{p}=1}^{4}\eta_{\mathrm{p}}^4+\frac{1}{6}A_3^{\mathrm{R}}\left(\sum_{\mathrm{p}=1}^{4}\eta_{\mathrm{p}}^2\right)^3 \tag{15}$$

where $A_1^{\mathrm{R}}=4.66\times10^5$ Jm^{-3}K^{-1}, $A_2^{\mathrm{R}}=1.02\times10^7$ Jm^{-3} and $A_3^{\mathrm{R}}=1.195\times10^7$ Jm^{-3} [61] are the expansion coefficients. It is well documented that 1% variation in Ni concentration of the B2 parent phase could change the MT start temperature of R phase (R_{s}) by ~100 K [26,62]. By fitting the experimental data from the literatures [26,62], we obtained that $T_0=\begin{cases}310 & c_{\mathrm{Ni}}<50\ \mathrm{at.\%}\\310-100(c_{\mathrm{Ni}}-50) & c_{\mathrm{Ni}}\geq50\ \mathrm{at.\%}\end{cases}$.

The interaction free energy density is calculated as

$$f_{\mathrm{in}}^{\mathrm{R}}=\sum\nolimits_{\mathrm{i}=1}^{3}\sum\nolimits_{\mathrm{j}=1}^{3}-\sigma_{\mathrm{ij}}\cdot\varepsilon_{\mathrm{ij}}^{\mathrm{MT}} \tag{16}$$

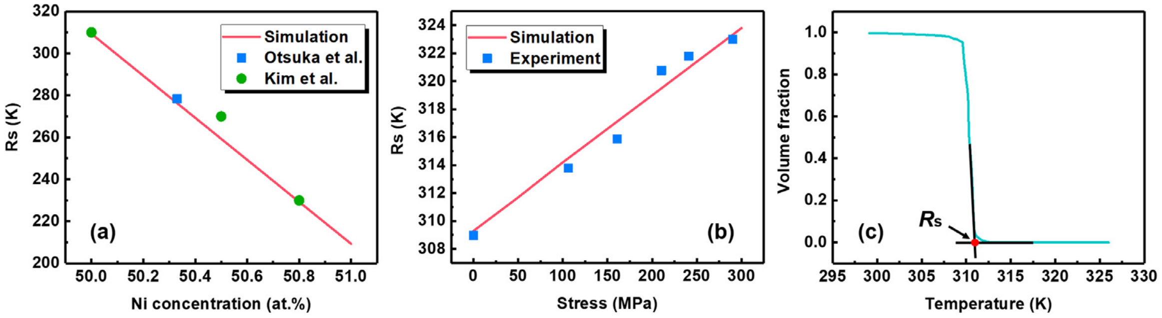

Fig. 1. Comparison between simulation and experimental results on (a) concentration-dependence of R_s and (b) stress-dependence of R_s in Ti-50.2at.%Ni aged at 773K for 900 s. Experimental data are from the literatures [14,26,72]. (c) Shows how R_s is determined in the simulations.

where σ_{ij} denotes the internal stress field induced by Ni_4Ti_3 precipitates in the matrix, and $\varepsilon^{\mathrm{MT}}_{\mathrm{ij}}=\sum_{\mathrm{p}=1}^{4}\varepsilon^{\mathrm{R}}_{\mathrm{ij}}(\mathrm{p})\eta^2_{\mathrm{p}}(\mathbf{r})$ is the strain field induced by R phase transformation in the matrix.

The last term in Eq. (14), $E^{\mathrm{R}}_{\mathrm{el}}$, is the coherency elastic strain energy of a structurally non-uniform but coherent system (i.e., martensitic variants coherently embedded in the parent phase matrix) characterized by $\eta_{\mathrm{p}}(\mathbf{r})$. $E^{\mathrm{R}}_{\mathrm{el}}$ can be calculated from Eq. (8) by substituting $\varepsilon^{\mathrm{P}}_{\mathrm{ij}}(\mathrm{p})$ and ϕ_{p} (p=1-8) with $\varepsilon^{\mathrm{R}}_{\mathrm{ij}}(\mathrm{q})$ and η_{q} (q=1-4), respectively.

2.2.3. Kinetic equation

The following time-dependent Ginzburg-Landau equation [49] is used to describe the temporal and spatial evolution of the structural order parameters during the MT

$$\frac{d\eta_{\mathrm{p}}(r,\ t)}{dt}=-L_{\eta}\frac{\delta F}{\delta\eta_{\mathrm{p}}(r,\ t)}+\xi_p(\mathbf{r},\ t),\ \ \mathrm{p}=1-4 \tag{17}$$

where $L_{\eta}=8.8\ \times 10^5\mathrm{m}^3\mathrm{J}^{-1}\mathrm{s}^{-1}$ [53] is the kinetic coefficient of MT, and $\xi_p(\mathbf{r},\ t)$ is the Langevin noise term that meets the following fluctuation-dissipation theorem [27,37]:

$$<\xi_p(\mathbf{r},\ t)\xi_p(\mathbf{r}',\ t')>=2\frac{k_BT}{|\Delta f|l^3}\delta(\mathbf{r}-\mathbf{r}')\delta(t-t') \tag{18}$$

where$\langle\rangle$ denotes the correlation of the Langevin noise term in space and time, k_B is the Boltzmann constant, T is the absolute temperature, $|\Delta f|$ is the chemical driving force, l is the length scale assigned to the computational grid increment, and δ is the delta function.

Eqs. (10), (11) and (17) are solved numerically in the reciprocal space using a finite difference method. To accelerate the nucleation process in the simulations, a relatively large amplitude of the Langevin noise term in Eq. (17) is first introduced, and then it is decreased by a factor of 10. The system size used in the simulations is $128l_0\times128l_0\times128l_0$ with $l_0=4$ nm. Periodical boundary conditions are applied along all three dimensions. The phase field model of MT is validated by comparing the simulated R_s of different compositions and R_s under different externally applied stress with corresponding experimental results, as shown in Fig. 1(a) and (b). The simulated R_s is determined via tangent method as illustrated in Fig. 1(c). It is readily seen that the simulation results agree with experimental results well.

3. Results

3.1. Ni concentration gradient in B2 matrix created by precipitation

It is well documented that the composition has a strong influence on MTs in NiTi SMAs [14,63]. It is also reported that a Ni_4Ti_3 precipitate could induce Ni concentration gradient in surrounding matrix [64]. Note that, in this study, the Ni concentration gradient refers to the spatially non-uniform distribution of Ni in the B2 matrix created by Ni_4Ti_3 precipitation, instead of the composition difference between the coexisting B2 and Ni_4Ti_3 phases. Fig. 2 shows the evolution of the concentration field in the B2 matrix induced by the growth of a single Ni_4Ti_3 precipitate in Ti-50.3at.%Ni during ageing at 723K. It is readily seen that the growth of the Ni_4Ti_3 precipitate creates a Ni depletion region around it (see Fig. 2(c)). As ageing time extends, the Ni depletion region becomes larger in size and lower in Ni concentration (see Fig. 2(b)–(f)) and eventually the entire matrix reaches its equilibrium concentration (Fig. 2(h)) when the precipitate phase reaches its equilibrium volume fraction. Since the thermodynamic stability of the R phase depends sensitively on Ni concentration of the B2 phase, its variation will have a strong influence on the MT behavior as will be shown below.

3.2. Effect of ageing time on MT

Fig. 3(a) and (b) show the variation of one dimensional (1D) concentration profile of Ni with ageing time in the system shown in Fig. 2. In consistence with Fig. 2, Ni valley first forms at the vicinity of the precipitate and becomes deeper and wider as ageing time increases. At equilibrium, the concentration of Ni in the B2 matrix reaches 50 at.%, much lower than its initial value of 50.3 at.%. Corresponding to the Ni concentration variation in the B2 matrix, the MT behavior changes dramatically as shown in Fig. 3(c). In the system with small Ni concentration variation (see the t=630s one), the MT occurs abruptly in a narrow temperature interval, which is a typical characteristic of a strong first-order phase transition. Interestingly, as the concentration heterogeneity develops, the MT starts at higher temperatures and occurs within a wider temperature range (see ageing time t=2898s ~ 8190s), showing a slow and continuous increase in martensite volume fraction (a characteristic of a high-order transition) followed by a more rapid increase (the characteristic of a first-order transition) upon cooling. It should be point out that the R phase transformation remains to be first-order in nature although a continuous increase of the R phase volume fraction within a certain temperature range has been observed in Fig. 3(c). This apparent continuous transformation actually consists of a series of consecutive local martensitic transformation events in the Ni concentration gradient in the B2 matrix phase created by the Ni_4Ti_3 precipitate. Further ageing leads to the temperature window of MT gradually narrows down again. When the precipitate has reached its equilibrium volume fraction, Ni concentration in the B2 matrix becomes uniform again and the system exhibits a characteristic of a strong first-order MT with a higher R_s (see t=17262s). Quantitative analysis of the curves shown in Fig. 3(c) leads to Fig. 3(d), which shows the variations of the temperature range for the MT (the green curve) and R_s (the blue curve)

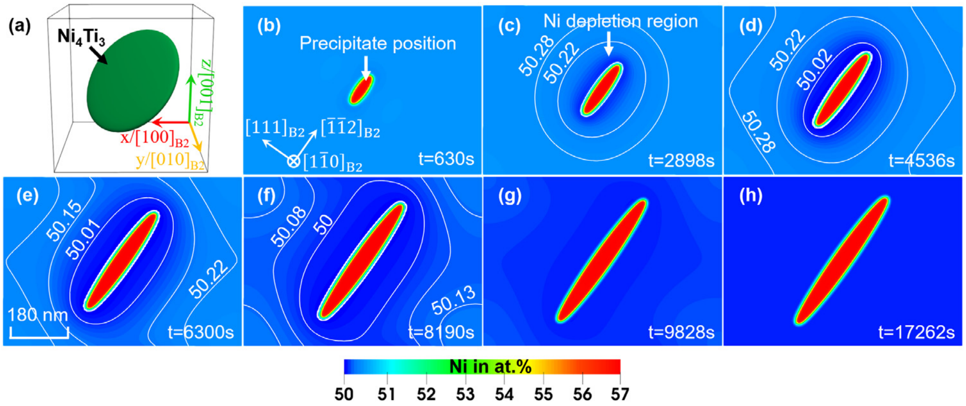

Fig. 2. (a) Three dimensional view of a Ni_4Ti_3 precipitate (variant 1). (b)–(h) Evolution of the concentration field of Ni in the B2 matrix around a Ni_4Ti_3 precipitate (variant 1) on the $(1\bar{1}0)_{B2}$ cross-section plane going through the center of the precipitate. The corresponding ageing time is marked on the bottom-right corner of each panel figure. The Ni concentration marked in (c)–(f) has a unit of at.%.

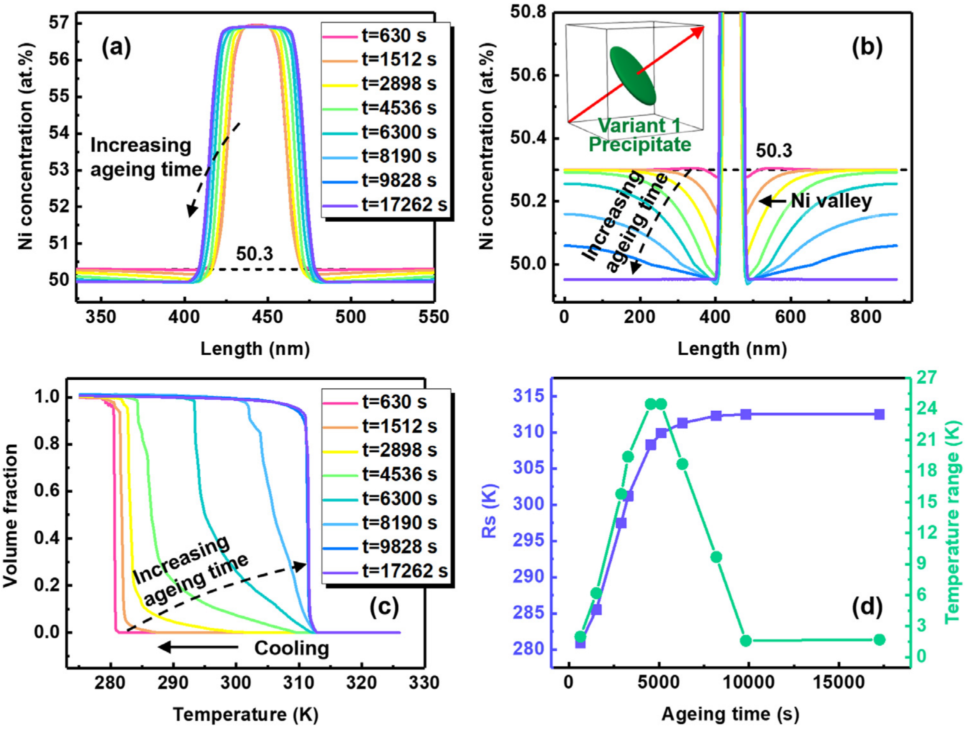

Fig. 3. (a) Concentration profile of Ni at different ageing times along the red line going through the center of the precipitate on the $[111]_{B2}$ direction, i.e. the thickness direction of variant 1, (see the inset in (b)). (b) Enlarged concentration profile of Ni at different ageing times. Note that (a) and (b) share the same legend. (c) Variation of volume fraction of martensite upon cooling in systems shown in (a). (d) Evolution of R_s and the temperature window size of MT with ageing time.

with ageing time. As the ageing time increases, the temperature window size for the MT first increases and then reaches a maximum before it comes back down to the original level (but corresponding to a much higher R_s). The R_s rapidly increases with ageing time before it finally reaches a plateau. This is consistent with the experimental result in the literature [26]. The variation of R_s is directly related to the change of the relative thermodynamic stability between the parent and R phases. Ni_4Ti_3 precipitation alters the composition of the B2 matrix and creates local stress fields, both of which affect the thermodynamic stabilities of the parent and R phases. It will be shown later that the composition change plays the dominant role. Fig. 3(b) shows clearly that the Ni concentration decreases gradually in the vicinity of the Ni_4Ti_3 precipitate as ageing proceeds. Fig. 1(a) indicates that a lower Ni concentration in NiTi alloys leads to a higher R_s in the composition range showed. Therefore, the increase of R_s with ageing time shown in Fig. 3(d) originates from the decrease of Ni content in the B2 matrix caused by Ni_4Ti_3 precipitation.

3.3. MT in systems with different alloy compositions

In addition to ageing time at a fixed alloy composition, the alloy composition also influences the Ni concentration field around the precipitate at a fixed size, as demonstrated in Fig. 4 and Fig. 5(a). Note that all precipitates shown in Fig. 4 have the same size (achieved by controlling the ageing time) and, thus, the difference in coherency stresses is minimized. Fig. 4 shows the concentration field of Ni in five different alloys. It is obvious that a higher initial Ni concentration in the alloy leads to a larger Ni concentration heterogeneity in the B2 matrix, which appears as steeper and deeper Ni valley in Fig. 5(a). As the Ni valley becomes steeper and deeper, the MT changes from a strong first-order to a mixture of apparent

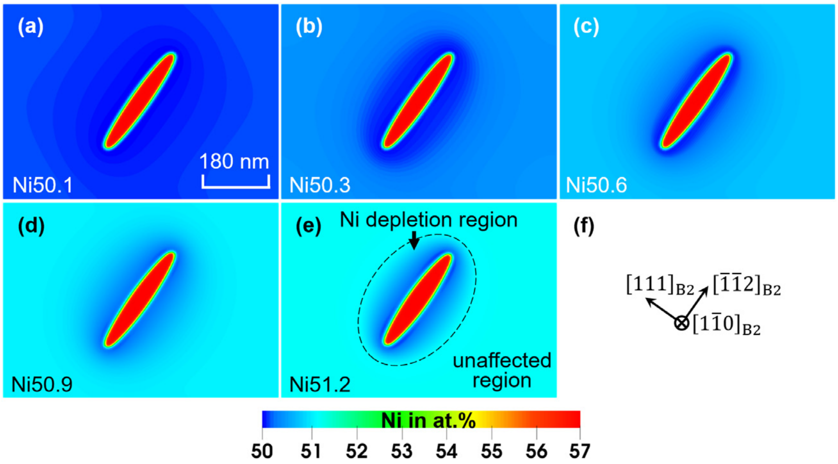

Fig. 4. Ni concentration field around a growing Ni_4Ti_3 precipitate on the $(1\bar{1}0)_{B2}$ cross-section plane going through the center of the precipitate in five different alloys with initial Ni concentration of (a) 50.1 at.%, (b) 50.3 at.%, (c) 50.6 at.%, (d) 50.9 at.% and (e) 51.2 at.%. Note that all precipitates in this figure has the same size. The dashed ellipse in (e) highlights the Ni depletion region. (f) Shows the crystallographic orientation of the cross-section plane.

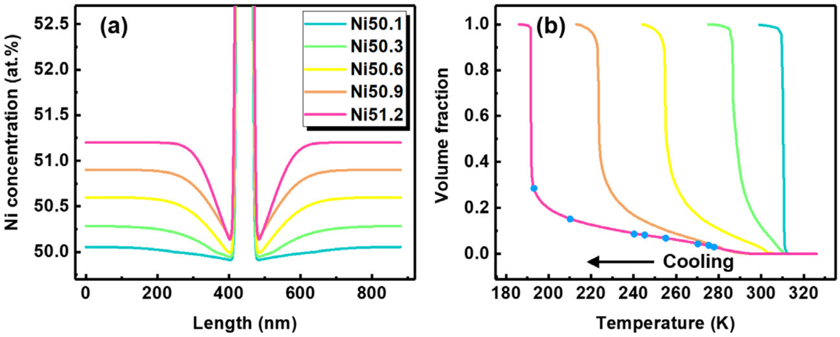

Fig. 5. (a) Concentration profile of Ni of the five alloys shown in Fig. 4. Curves are plotted along the line going through the center of the precipitate in the $[111]_{B2}$ direction as shown in the upper-left inset of Fig. 3. (b) Variation of volume fraction of martensite upon cooling obtained for the five alloys shown in (a). (b) share the same legend with (a). The blue dots in (b) mark locations of the panel figures in Fig. 6. (For interpretation of the references to color in this figure legend, the reader is referred to the web version of this article.).

continuous followed by a strong first-order as shown in Fig. 5(b). It will be shown later that the apparent continuous phase transition behavior corresponds to MT occurred in the Ni depletion region and the subsequent first-order phase transition corresponds to MT in the unaffected region.

4. Discussion

4.1. Effects of Ni concentration gradient in B2 matrix and coherency stress associated with precipitation on MT

It is generally accepted that a Ni_4Ti_3 precipitate could induce both Ni concentration gradient and internal stress field in the B2 matrix, both of which promote the MT at the interface between the precipitates and the B2 matrix [30]. In this section, the roles played by the concentration field and internal coherency stress field associated with Ni_4Ti_3 precipitation are analyzed by taking Ti-51.2at.%Ni as an example. Fig. 6 shows the microstructure evolution during MT in the system shown in Fig. 4(e), and each microstructure shown in Fig. 6 is at its equilibrium state of corresponding temperature. It is readily seen that, upon cooling, the R phase first appears at the interface between the B2 matrix and the Ni_4Ti_3 precipitate because of the following reasons: (i) the lowest Ni concentration resides in this region (see Fig. 5(a)) (note that a lower Ni concentration corresponds to a higher R_s as shown in Fig. 1(a)); (ii) the internal stress associated with the Ni_4Ti_3 precipitate, which assists the B2 to R martensitic transformation, peaks in the vicinity of the interface (see Fig. 7). This is consistent with the experimental observations [17,24,65]. Moreover, Fig. 6(g1) and (h1) show obvious variant preference in different parts of the precipitate due to variant selection by the internal coherency stress as shown in Fig. 6(b) and (d). The R phase variant selection by the internal coherency stress field shown in Fig. 6(b) and (d) is determined by calculating the elastic interaction energy associated with the nucleation of a R phase variant in the stress field generated by Ni_4Ti_3 precipitates. A variant is preferred if its interaction energy has a negative value. Under the influence of autocatalysis, further growth leads to different internally twinned structures in different parts of the precipitate-matrix interface, as shown in Fig. 6(g2)–(g8). This indicates that the internal stress plays a dominant role in determining self-accommodating patterns of martensitic domains.

Another feature of the MT shown in Fig. 6 is the gradual growth of martensitic domains in a wide temperature range, which is in sharp contrast to the conventional first-order R phase transformation. From the thermodynamics' point of view, a gradual growth of martensites upon cooling indicates a spatial heterogeneity in relative thermodynamic stability of the B2 matrix and R martensitic phases. In the studied system, it is straightforward to conceive the contribution of compositional non-uniformity to the phase-stability heterogeneity because R_s is a strong function of composition as shown in Fig. 1(a). While, it should be noted that the internal coherency stress field from the Ni_4Ti_3 precipitate contributes to the phase stability heterogeneity as well, as Fig. 8(a) shows. To clarify the contributions made by concentration field and co-

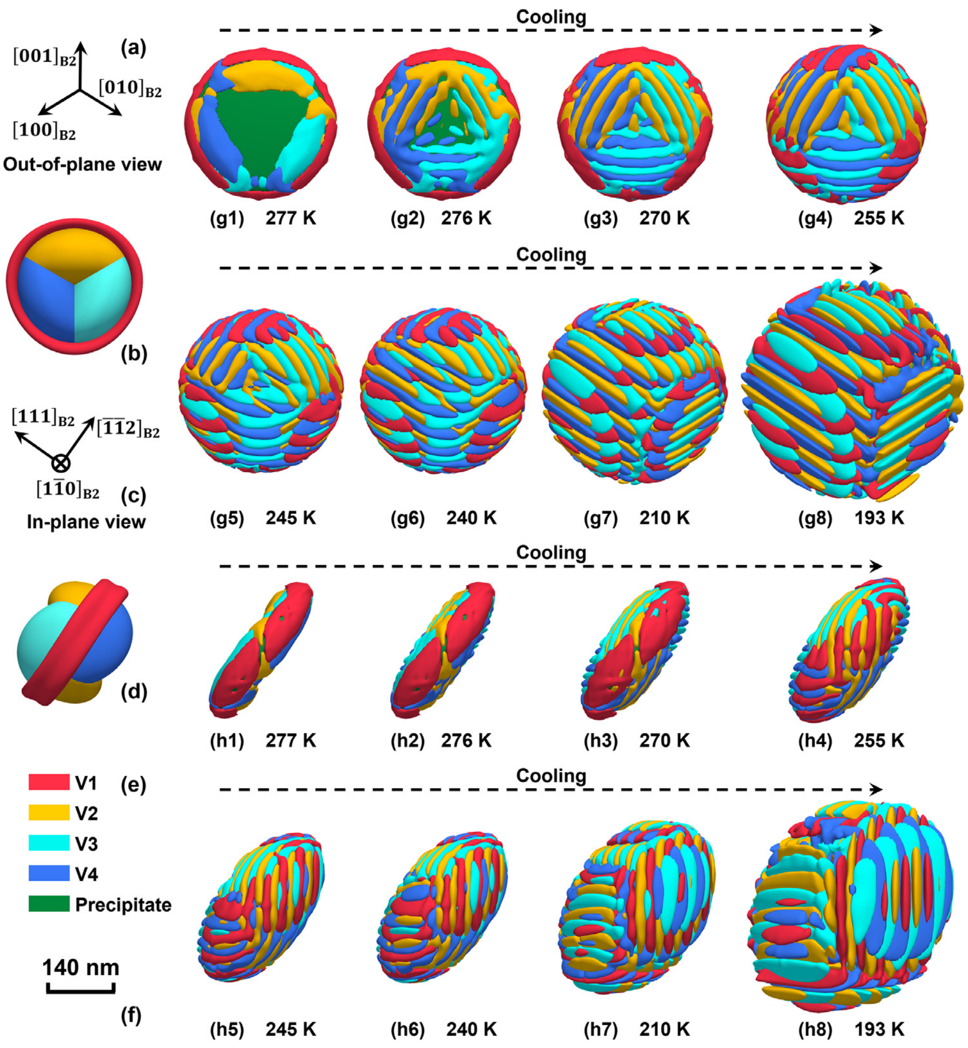

Fig. 6. Microstructure evolution process during MT upon cooling in the alloy shown in Fig. 4(e). (a) shows the viewing angle of (b) and (g1)–(g8), and (c) shows the viewing angle of (d) and (h1)–(h8). These two viewing angles are termed as out-of-plane and in-plane views, respectively. (b) and (d) show the R phase variants preferred by the internal stress accompanying the Ni_4Ti_3 precipitate. (g1)–(g8) and (h1)–(h8) show the out-of-plane and in-plane view of the martensitic microstructure evolution upon cooling, respectively. Four R phase variants (abbreviated as V1, V2, V3 and V4) and the precipitate are represented by different colors as shown in (e). (f) is the length scale of microstructures shown in (g1)–(g8) and (h1)–(h8). The locations of (g1)–(g8) and (h1)–(h8) on the volume-temperature curve are marked by the blue dots in Fig. 4(e). (For interpretation of the references to color in this figure legend, the reader is referred to the web version of this article.).

herency stress field associated with a precipitate to the phase stability heterogeneity of the B2 matrix phase with respect to its transformation to R martensite, a quantitative comparison between the chemical driving force and internal stress driving force is given in Fig. 8(b). It is found that the internal stress driving force is smaller than the chemical driving force even at the beginning (277 K) of MT when the latter is the smallest. This indicates that the Ni concentration gradient in the B2 matrix dominates the apparent continuous MT behavior upon cooling. This is consistent with previous studies [4–7]. To further validate this result, a comparison study, in which the effect of internal stress is not considered, is performed as shown in Fig. 8(c). It is readily seen that the MT remains apparent continuous even without considering the influence of the internal coherency stress field although the R_s shifts slightly to a lower temperature. This demonstrates that the internal stress has an apparent influence on MT only at the beginning of MT when the chemical driving force is relatively small. Therefore, we can safely draw a conclusion that the Ni concentration gradient in the B2 matrix produced by Ni_4Ti_3 precipitation in this alloy is responsible for the apparent continuous behavior of the MT.

It should be pointed out that the contribution of the Ni concentration gradient and internal coherency stress to the driving force of MT shown in Fig. 8(b) is for the case of a single precipitate in the periodically repeating computational cell. For systems with nanoscale precipitates, intensive internal coherency stress fields should be created by densely populated precipitates, which alters the contribution of internal stress fields to the driving force of MT. In this case, the internal stress field may also influence significantly the kinetic process of MT, as reported in the literature [66].

4.2. Precipitation–an effective way of tuning MT

It is well known that SMAs with narrow hysteresis and controllable strain release are desired in a rich variety of functional and biomedical applications. However, the strong first-order nature of MTs makes SMAs show large hysteresis and strong nonlinear stress strain behavior. It is reported that nanoscale concentration modulations in the parent B2 phase are effective ways of tuning MTs [4–7]. While the fabrication of materials with desired nanoscale concentration modulations remains challenging, results

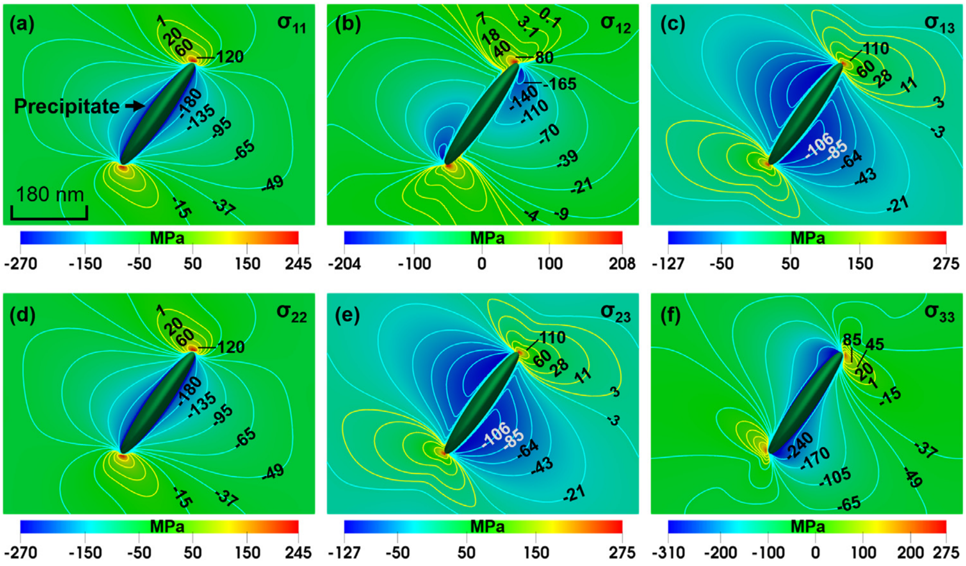

Fig. 7. Internal stress field induced by a Ni_4Ti_3 precipitate on the $(1\bar{1}0)_{B2}$ cross-section plane going through the center of the precipitate. The yellow and cyan curves in each panel figure are contour lines with positive and negative stress values, respectively. The deep green particle at the center of each panel figure is the precipitate. Note that the precipitate in this figure is the one shown in Fig. 4(e). (For interpretation of the references to color in this figure legend, the reader is referred to the web version of this article.).

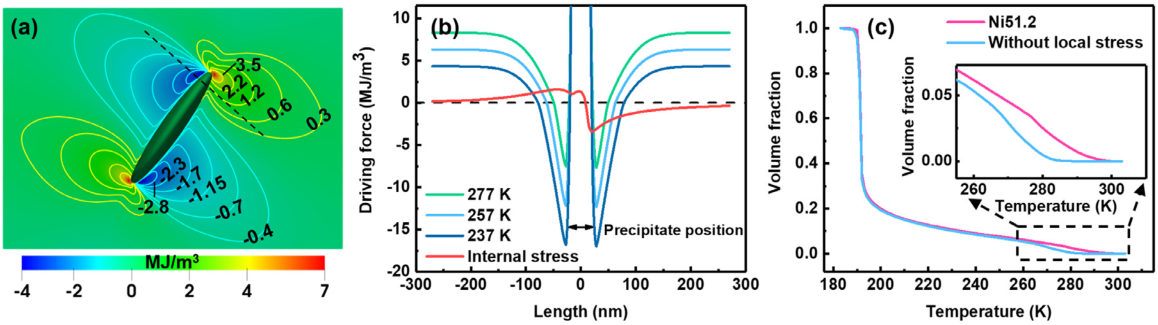

Fig. 8. (a) Driving force for MT contributed by coherency stress (termed as internal stress driving force) to variant 2 of R phase on the $(1\bar{1}0)_{B2}$ cross-section plane going through the center of the precipitate, which is calculated via Eq. (16). A negative value promotes the R phase transformation, while a positive value means the opposite. (b) Internal stress driving force and chemical driving force at different temperatures along the dashed line shown in (a). The chemical driving force is defined as $\Delta f_{ch} = f_{ch}(\text{Martensite}) - f_{ch}(\text{Austenite})$. (c) Comparison in volume fraction of martensite upon cooling between systems with and without the influence of internal stress.

shown in Section 4.1 indicates that the concentration gradient generated by precipitation, which is responsible for the apparent continuous part of the MT, is promising in tailoring the MT behavior. For example, the variation of concentration gradient in degree and extent shown in Fig. 3(b) results in dramatic change of the MT behavior shown in Fig. 3(c). Particularly, the concentration profile generated at t=9828 s leads to a gradual and almost linear increase in volume fraction of martensite upon cooling, which is desired in practical applications [1]. Besides the concentration gradient, the internal stress field associated with the precipitates has a potential to tune the MT behavior as well. It has been reported that the internal stress fields accompanying point defects [8], dislocations [9], and nanoprecipitates [66] transform the otherwise first-order MT to an apparent continuous MT. This indicates that the kinetic process of MT can be tailored by designing an internal stress field via controlling the microstructure of precipitates. Moreover, Figs. 3(b) and 5(b) clearly demonstrate that the MT behavior can be effectively tailored via adjusting the ageing time and tuning the Ni concentration field in the B2 matrix. Therefore, it is promising to develop a simple, general, and low-cost way of fabricating high-performance SMAs with desired properties by precipitation.

4.3. Effect of multiple precipitates

Precipitates generated during ageing may form complex microstructures as shown in Fig. 9. The relative position and orientation between neighboring precipitates can be categorized primarily into 3 types: (i) parallel with each other plus an offset on the in-plane direction of precipitates, e.g., particle 1 and particle 2 in Fig. 9(b); (ii) one precipitate ends at the center of another precipitate (termed as type-I intersection), e.g., particle 1 and particle 3; and (iii) two precipitates meet at the ends (termed as type-II intersection), e.g. particle 4 and particle 5. Below, we will discuss MTs in systems with these 3 types of “building blocks” of a complex precipitate microstructures. Note that the n-th variant of precipitate and R phases are abbreviated as PVn and Vn, respectively.

4.3.1. MT in systems with parallel precipitates

Fig. 10(a1)–(a6) show the internal stress field induced by two parallel precipitates. The coupling between the precipitates brings obvious change to the internal stress field as compared with the single precipitate case shown in Fig. 7. For example, the σ_{11}, σ_{12}, and σ_{22} are enhanced apparently in the region residing between precipitates. Additionally, Fig. 10(b) and (c) demonstrate that the

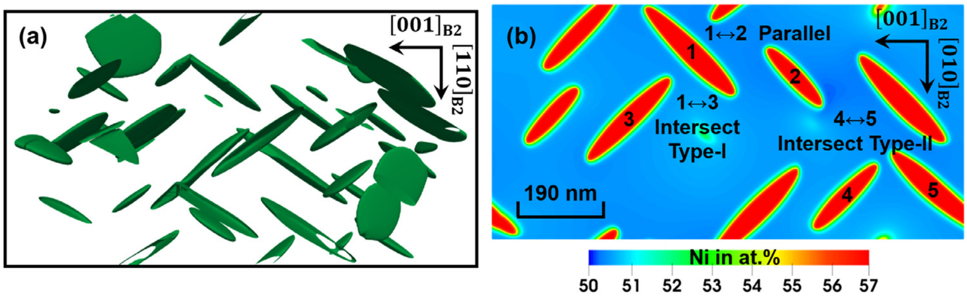

Fig. 9. (a) Three dimensional view of a microstructure formed by multiple Ni_4Ti_3 precipitates in Ti-51.3at.%Ni after ageing at 713K for 5708 s. (b) Two dimensional cross-section view of the microstructure shown in (a) on the $(100)_{B2}$ plane.

region residing between precipitates has a relatively low Ni concentration. These conditions make the MT start from the region between precipitates, as shown in Fig. 10(e1). As temperature decreases, the martensitic domains grow first by filling up the region between the precipitates (see Fig. 10(e1)–(e3)) and then by encircling the precipitates (see Fig. 10(e4)–(e9)). Fig. 10(e1)–(e3) shows two features that are noteworthy: (i) the martensitic domain contains only V3 and V4 because of the strong variant selection process by the misfit stress in the corresponding region, (ii) the growth of the martensitic domain shows an apparent continuous behavior (Fig. 10(d)) and is well confined to the region between the precipitates. It is noteworthy that the rapid increase of volume fraction of martensites at lower temperatures shown in Fig. 10(d) can be transformed into slow increase just like at higher temperatures by designing the microstructure formed by Ni_4Ti_3 precipitates. The ability of selecting martensitic variants and regulating their growth leads to a potential to develop Invar alloys [67] by generating specific strain from the MT that counteracts the intrinsic thermal contraction of the crystals upon cooling [9,68,69]. For the system shown in Fig. 10(e1)–(e3), in which V3 and V4 have identical volume (see Fig. 10(d)), the average strain [68] of the martensitic domain is $\frac{1}{2}[\boldsymbol{\varepsilon}^{R}(3)+\boldsymbol{\varepsilon}^{R}(4)] = -0.001\begin{bmatrix} 0.2 & 6 & 0 \\ 6 & 0.2 & 0 \\ 0 & 0 & 0.2 \end{bmatrix}$ whose eigen-strain components are 0.0058, -0.0002 and -0.0063. With eigen-strains that are larger than the thermal expansion coefficient of the austenitic phase of NiTi alloys which is $\sim 1.1 \times 10^{-5}\ K^{-1}$ [70], the strains generated from R phase transformation are promising to compensate the intrinsic thermal contraction upon cooling by adjusting the strain release of MT via controlling the ageing process.

4.3.2. MT in systems with type-I intersecting precipitates

The internal stress induced by a single precipitate shown in Fig. 7 demonstrates that the stress decays faster on the in-plane direction of the Ni_4Ti_3 particle than on the out-of-plane direction. Therefore, in contrast to the parallel precipitates case, no large stress concentration region is observed in the microstructure formed by type-I intersecting precipitates although the stress field is enhanced as compared with the single precipitate case, as shown in Fig. 11(a1)–(a6). The concentration field shown in Fig. 11(b) and (c) indicates that the lowest Ni concentration appears near the intersecting point of precipitates, which agrees with the experimental report [64]. In response to the Ni distribution, the MT starts from the intersecting point upon cooling as Fig. 11(e1) shows. Further cooling makes martensitic domains grow at the vicinity of precipitates under the regulation of Ni concentration gradient (see Fig. 11(e2)–(e10)). The MT scenario of the microstructure formed by type-I intersecting is similar to the single precipitates case, which indicates that the coupling in internal stress and Ni concentration field between precipitates is relatively weak as compared with the parallel precipitates.

4.3.3. MT in systems with type-II intersecting precipitates

In contrast to type-I intersecting precipitates, obvious coupling of internal stress between precipitates is observed in the type-II intersecting microstructure. The coupling makes some stress components be reinforced (see Fig. 12(a1), (a2), (a4) and (a6)) and some stress components be reduced (see Fig. 12(a3) and (a5)). Additionally, Fig. 12(a1)–(a6) indicate that the coupling decays as the distance between precipitates increases. Fig. 12(b) and (c) demonstrate that the region near the intersecting point possesses the lowest Ni concentration, and Ni concentration gradually increase as apart from the intersecting point. Upon cooling, the MT initiates from the intersecting point by forming an internally-twinned structure as shown in Fig. 12(e1). As temperature decreases, the martensitic domains grow in a similar way as we observed previously in the parallel precipitates, i.e. first filling up the region between precipitates and then encircling precipitates (see Fig. 12(e2)–(e10)). It is noteworthy that, at the beginning of MT, the martensitic domain contains only V3 and V4 of R phase because of the variant selection effect of internal stress (see Fig. 12(e1) and (e2)). The variant selection phenomenon of type-II intersecting precipitates also provides an opportunity to develop invar effect based on aged NiTi SMAs.

It is noteworthy that microstructures formed by parallel and intersecting precipitates exhibit similar apparent continuous MT at the initial stage of MT although the relative orientation of precipitates are different in them, as demonstrated by Figs. 10(d), 11(d) and12(d). This indicates that the MT behavior is not sensitive to the orientation of precipitates, which agrees with the experimental report [24]. The reason behind this phenomenon is that the apparent continuous behavior of MT is mainly determined by Ni concentration gradient that can be induced by all precipitate variants. The difference in relative orientation among Ni_4Ti_3 particles may alter the structure of martensitic domains because of the variant selection effect of internal stress field, but it does not influence the MT behavior.

4.3.4. Limitation of simulations

To get a system with a single Ni_4Ti_3 precipitate that is presented in Fig. 2, a Ni_4Ti_3 particle of 16 nm with its equilibrium composition is introduced into a uniform B2 matrix with an initial composition of 50.3at.%Ni at the beginning (i.e., t=0 s) of the simulation. This way of introducing the precipitate leads to a transition period from the artificial initial configuration introduced at the beginning till the system establish local-equilibrium at the interface. While, microstructures shown in Fig. 2 are after the transition period, and, thus, reflect the real evolution process of concentration field.

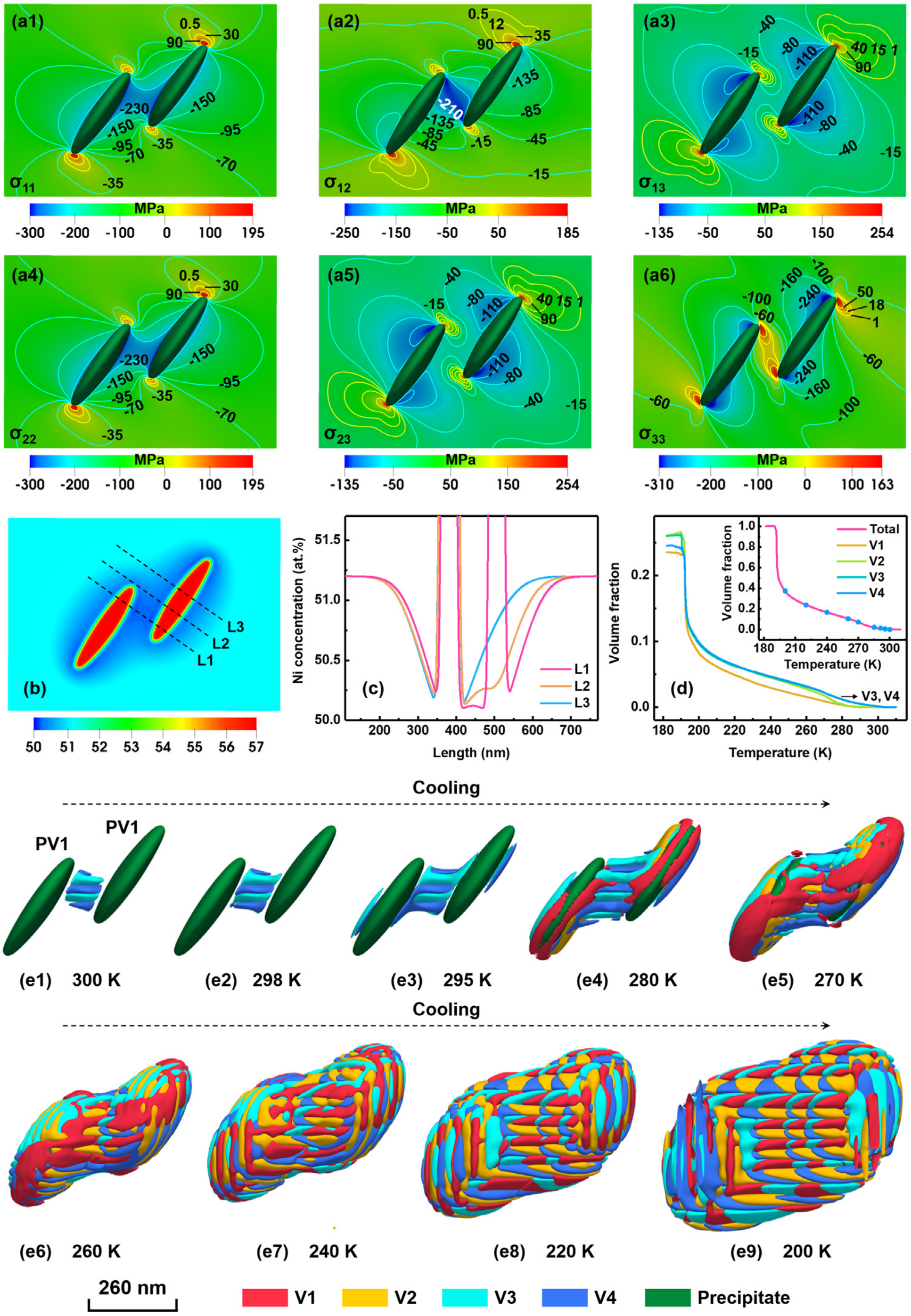

Fig. 10. (a1)–(a6) show the internal stress field induced by parallel Ni_4Ti_3 precipitates on the $(1\bar{1}0)_{B2}$ cross-section plane going through the center of the precipitates. (b) shows the concentration field of Ni on the $(1\bar{1}0)_{B2}$ cross-section plane. (c) plots the concentration profiles of Ni along the three dashed lines in (b), i.e., L1, L2 and L3. (d) Variation of volume fraction of each R martensite variant upon cooling. The inset in (d) shows the total volume fraction of martensite, i.e., the sum of volume fractions of the 4 variants. (e1)–(e10) Microstructure evolution process during MT upon cooling. The locations of (e1)–(e10) on the volume-temperature curve are marked by the blue dots in (d). (For interpretation of the references to color in this figure legend, the reader is referred to the web version of this article.).

Five alloys with different initial compositions shown in Figs. 4 and 5(a) are aged at the same temperature 723K, thus all the alloys should have the same local equilibrium Ni concentration at the interface. However, Ni concentration profiles shown in Fig. 5(a) exhibit different Ni concentrations at the interface between Ni_4Ti_3 precipitates and the matrix. This is because precipitates shown in Figs. 4 and 5(a) have not reached the local-equilibrium yet at the interface to make them have the same size to minimize the difference in internal coherency stresses.

5. Summary

In summary, the precipitate microstructure evolution during ageing and the influence of compositional non-uniformity and internal coherency stress field in the B2 matrix phase on R martensitic transformation in several Ni-rich NiTi shape memory alloys (SMAs) are investigated using phase field simulations. The main findings are summarized as follows:

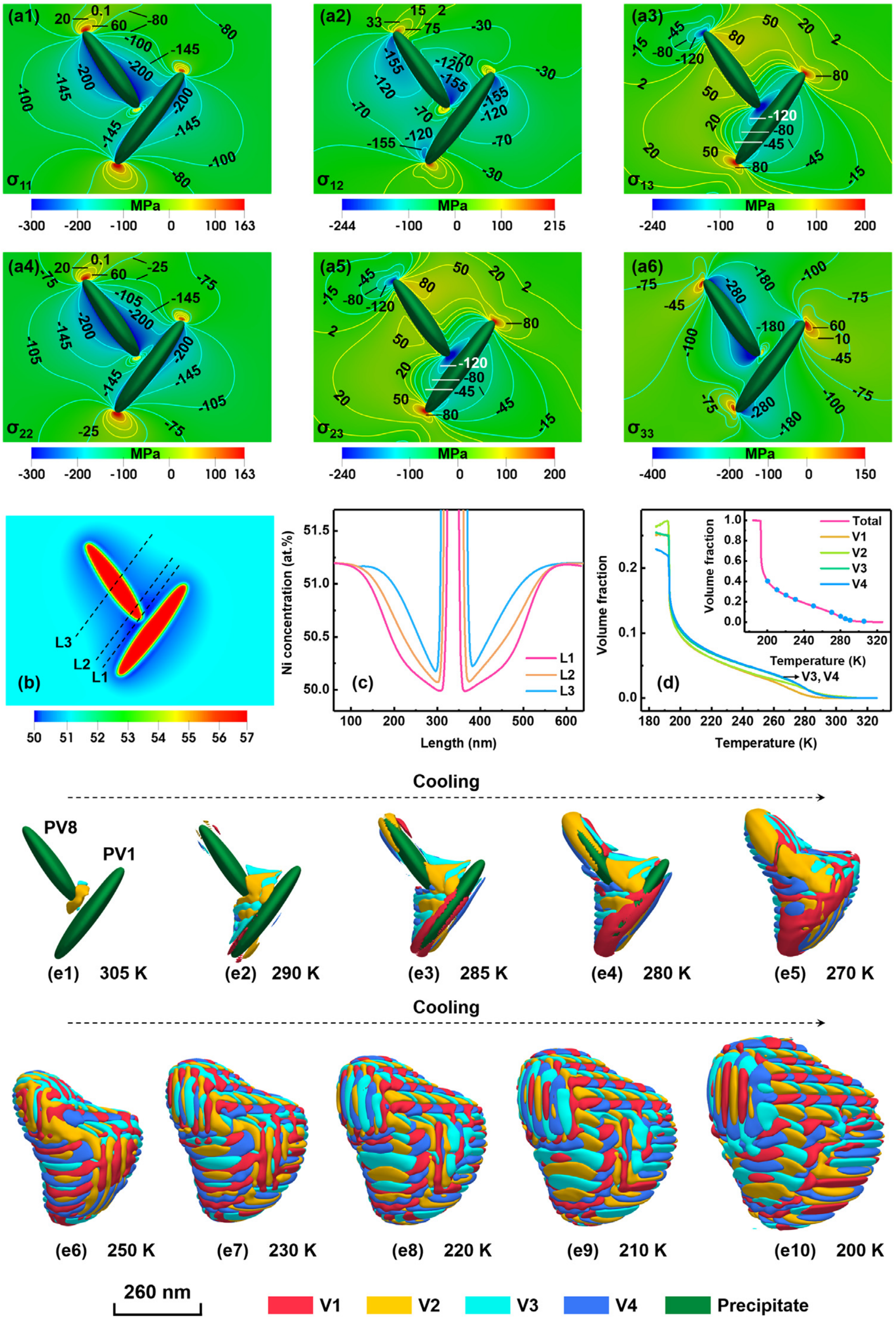

Fig. 11. (a1)–(a6) show the internal stress field induced by variant 1 (PV1) and variant 8 (PV8) of Ni_4Ti_3 precipitates on the $(1\bar{1}0)_{B2}$ cross-section plane. (b) shows the concentration field of Ni on the $(1\bar{1}0)_{B2}$ cross-section plane. (c) plots the concentration profiles of Ni along the three dashed lines in (b), i.e., L1, L2 and L3. (d) Variation of volume fraction of each R martensite variant upon cooling. The inset in (d) shows the total volume fraction of martensite, i.e., the sum of volume fractions of the 4 variants. (e1)-(e10) Microstructure evolution process during MT upon cooling. The locations of (e1)-(e10) on the volume-temperature curve are marked by the blue dots in (d). (For interpretation of the references to color in this figure legend, the reader is referred to the web version of this article.).

(i) Ni_4Ti_3 precipitates cause Ni concentration gradient in the B2 matrix by forming Ni-depletion regions around the precipitates. The degree and extent of the Ni concentration gradient in the B2 matrix can be controlled by ageing time and alloy composition. As a result, the behavior of R phase transformation undergoes a first-order → apparent continuous followed by first-order → first-order transition as a function of the ageing time.

(ii) A higher initial Ni concentration makes the Ni concentration gradient stronger in degree and thus leads to a wider temperature window for the R phase transformation.

(iii) Ni concentration gradient plays the main role in determing the kinetic process of the martensitic transformation (MT) and is responsible for its apparent continuous behavior, while the internal stress field induced by the precipitates dictates the

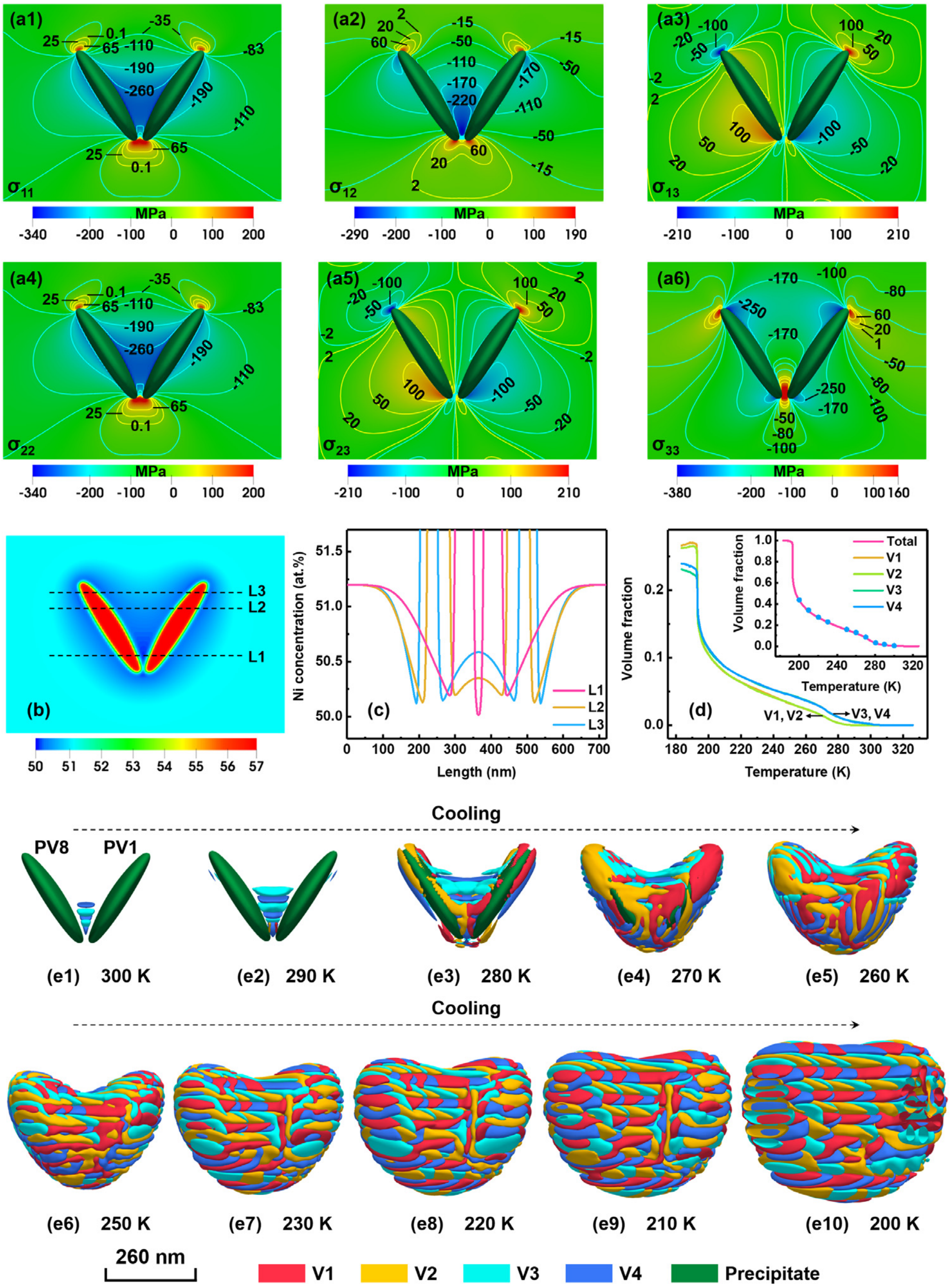

Fig. 12. (a1)–(a6) sShow the internal stress field induced by variant 1 (PV1) and variant 8 (PV8) of Ni_4Ti_3 precipitates on the $(1\bar{1}0)_{B2}$ cross-section plane. (b) shows the concentration field of Ni on the $(1\bar{1}0)_{B2}$ cross-section plane. (c) plots the concentration profiles of Ni along the three dashed lines in (b), i.e., L1, L2 and L3. (d) Variation of volume fraction of each R martensite variant upon cooling. The inset in (d) shows the total volume fraction of martensite, i.e., the sum of volume fractions of the 4 variants. (e1)–(e10) Microstructure evolution process during MT upon cooling. The locations of (e1)–(e10) on the volume-temperature curve are marked by the blue dots in (d). (For interpretation of the references to color in this figure legend, the reader is referred to the web version of this article.).

internally-twinned structure of martensitic domains via variant selection.

(iv) Typical "building blocks" of a complex multi-precipitate microstructure are identified. Internal stress, Ni concentration gradient, and R phase transformation in systems with each individual building block are investigated. For parallel precipitates, it is found that the MT starts from regions residing in between the parallel precipitates and that this structure has a strong variant selection effect and a strong confinement of the growth of martensitic domains. For intersecting precipitates, however, the MT initiates from the intersecting point. Parallel precipitates and type-II intersecting precipitates exhibit a strong variant selection effect.

(v) The ability of precipitates in selecting martensitic variants and regulating their growth makes it possible to develop Invar and Elinvar alloys by tailoring precipitate microstructures via the Ni concentration gradient and internal stress field.

(vi) The effectiveness of Ni concentration gradient and stress field associated with nanoprecipitates in changing MT behavior indicates that precipitation provides a simple, general, and low-cost method for developing high-performance SMAs.

Declaration of Competing Interest

The authors declare no competing financial interests.

Acknowledgment

Jiaming Zhu acknowledges the support of Qilu Young Talent Program from Shandong University. Jiaming Zhu and San-Qiang Shi acknowledge the financial supports of the PolyU Post-Dr Research Grant (No. G-YW5T) from The Hong Kong Polytechnic University. Hong-Hui Wu acknowledges the National Natural Science Foundation of China (No. 51901013 and 52071023). YW acknowledges the support from U.S. National Science Foundation (Grant No. DMR-1923929).

Appendix

Magnitude of parameters in the phase field model of precipitation [41,43,71]:

$$G_{\mathrm{Ni}}^{\mathrm{bcc},0} = 3535.925 + 114.298T - 22.096T\ln T - 0.0048407T^2 (298.15\mathrm{K} < T < 1728\mathrm{K})$$

$$G_{\mathrm{Ti}}^{\mathrm{bcc},0} = -1272.064 + 134.786T - 25.5768T\ln T - 0.0006638T^2 - 2.788 \times 10^{-7}T^3 + 7208T^{-1} (298.15\mathrm{K} < T < 1155\mathrm{K})$$

$$G_{\mathrm{Ni:Ti}} = G_{\mathrm{Ti:Ni}} = -31000 + 11T$$

$$L^0_{\mathrm{Ni:Ni,Ti}} = L^0_{\mathrm{Ni,Ti:Ni}} = -56500 + 23T$$

$$L^1_{\mathrm{Ni:Ni,Ti}} = L^1_{\mathrm{Ni,Ti:Ni}} = 13500 - 8T$$

$$L^2_{\mathrm{Ni:Ni,Ti}} = L^2_{\mathrm{Ni,Ti:Ni}} = 37300 - 14T$$

$$L^0_{\mathrm{Ti:Ni,Ti}} = L^0_{\mathrm{Ni,Ti:Ti}} = 70000 - 13T$$

$$L^1_{\mathrm{Ti,NiTi}} = L^1_{\mathrm{NiTi,Ti}} = -10000 + 8T$$

$A_1 = -4.2749, A_2 = 4.8734, A_3 = -265001.2461, A_4 = -6, A_5$
$0, A_6 = 0.0175, A_7 = -3 \times 10^{-7}, A_8 = 609713,$

$$G_{\mathrm{Ti}}^{\mathrm{hcp},0} = -8059.921 + 133.615208T - 23.9933T\ln T - 4.777975 \times 10^{-3}T^2 + 0.106716 \times 10^{-6}T^3 + 72636T^{-1} (298.15\mathrm{K} < T < 900\mathrm{K})$$

$$G_{\mathrm{Ni}}^{\mathrm{fcc},0} = -5179.159 + 117.854T - 22.096T\ln T - 4.8407 \times 10^{-3}T^2 + G_{\mathrm{Ni}}^{\mathrm{mag}} + G_{\mathrm{pres}} (298.15\mathrm{K} < T < 1728\mathrm{K})$$

$$G_{\mathrm{Ni}}^{\mathrm{mag}} = RT\ln(B_0 + 1)g_1(\tau)$$

$$\tau = \frac{T}{T_{\mathrm{c}}}$$

$B_0 = 0.52,\ T_{\mathrm{c}} = 633\mathrm{K}$ for FCC Ni

$$g_1(\tau) = \begin{cases} 1 - \frac{1}{D}\left[\frac{79\tau^{-1}}{140p} + \frac{474}{497}\left(\frac{1}{p} - 1\right)\left(\frac{\tau^3}{6} + \frac{\tau^9}{135} + \frac{\tau^{15}}{600}\right)\right], & (\tau \le 1) \\ -\frac{1}{D}\left(\frac{\tau^{-5}}{10} + \frac{\tau^{-15}}{315} + \frac{\tau^{-25}}{1500}\right), & (\tau > 1) \end{cases}$$

$$D = \frac{518}{1125} + \frac{11692}{15975}\left(\frac{1}{p} - 1\right),\ p = 0.4 \text{ for BCC phase},\ 0.28 \text{ for others}$$

$$G_{\mathrm{pres}} = AP\left(1 + a_0T + \frac{a_1T^2}{2} + \frac{a_2T^3}{3} + a_3T^{-1}\right)$$

$A = 6.533939 \times 10^{-6}, P = 101325$ Pa,
$a_0 = 3.103614 \times 10^{-5}, a_1 = 2.418404 \times 10^{-8}$

References

[1] J. Mohd Jani, M. Leary, A. Subic, M.A. Gibson, A review of shape memory alloy research, applications and opportunities, Mater. Des. 56 (2014) 1078–1113.
[2] N. Morgan, Medical shape memory alloy applications—the market and its products, Mater. Sci. Eng. A. 378 (2004) 16–23.
[3] Y. Haga, M. Esashi, S. Maeda, Bending, torsional and extending active catheter assembled using electroplating, in: Proc. IEEE Thirteen. Annu. Int. Conf. Micro Electro Mech. Syst. (Cat. No.00CH36308), IEEE, 2000, pp. 181–186.
[4] J. Zhu, Y. Gao, D. Wang, T.-Y. Zhang, Y. Wang, Taming martensitic transformation via concentration modulation at nanoscale, Acta Mater. 130 (2017) 196–207.
[5] J. Zhu, D. Wang, Y. Gao, T.-Y. Zhang, Y. Wang, Linear-superelastic metals by controlled strain release via nanoscale concentration-gradient engineering, Mater. Today. 33 (2020) 17–23.
[6] J. Zhu, Y. Gao, D. Wang, J. Li, T.-Y. Zhang, Y. Wang, Making metals linear super-elastic with ultralow modulus and nearly zero hysteresis, Mater. Horiz. 6 (2019) 515–523.
[7] J. Zhu, H.-H. Wu, X.-S. Yang, H. Huang, T.-Y. Zhang, Y. Wang, S.-Q. Shi, Dissecting the influence of nanoscale concentration modulation on martensitic transformation in multifunctional alloys, Acta Mater. 181 (2019) 99–109.
[8] D. Wang, Y. Wang, Z. Zhang, X. Ren, Modeling abnormal strain states in ferroelastic systems: the role of point defects, Phys. Rev. Lett. 105 (2010) 205702.
[9] Y.C. Xu, C. Hu, L. Liu, J. Wang, W.F. Rao, J.W. Morris, A.G. Khachaturyan, A nano-embryonic mechanism for superelasticity, elastic softening, invar and elinvar effects in defected pre-transitional materials, Acta Mater. 171 (2019) 240–252.
[10] V.I. Levitas, M. Javanbakht, Interaction between phase transformations and dislocations at the nanoscale. Part 1. General phase field approach, J. Mech. Phys. Solids 82 (2015) 287–319.
[11] M. Javanbakht, V.I. Levitas, Interaction between phase transformations and dislocations at the nanoscale. Part 2: phase field simulation examples, J. Mech. Phys. Solids 82 (2015) 164–185.
[12] M. Javanbakht, M.S. Ghaedi, Nanovoid induced martensitic growth under uniaxial stress: effect of misfit strain, temperature and nanovoid size on PT threshold stress and nanostructure in NiAl, Comput. Mater. Sci. 184 (2020) 109928.
[13] N. Amigo, Martensitic transformation induced by void defects in the B2-CuZr crystal structure: an atomistic analysis, Mol. Simul. 45 (2019) 951–957.
[14] K. Otsuka, X. Ren, Physical metallurgy of Ti-Ni-based shape memory alloys, Prog. Mater. Sci. 50 (2005) 511–678.
[15] J.-S. Zhu, R. Gotthardt, New phase transition peak in NiTi alloy, Phys. Lett. A 132 (1988) 279–282.
[16] J. Zhang, W. Cai, X. Ren, K. Otsuka, M. Asai, The nature of reversible change in Ms temperatures of Ti-Ni alloys with alternating aging, Mater. Trans. JIM 40 (1999) 1367–1375.
[17] L. Bataillard, J.E. Bidaux, R. Gotthard, Interaction between microstructure and multiple-step transformation in binary NiTi alloys using in-situ transmission electron microscopy observations, Philos. Mag. A 78 (1998) 327–344.
[18] J. Khalil Allafi, X. Ren, G. Eggeler, The mechanism of multistage martensitic transformations in aged Ni-rich NiTi shape memory alloys, Acta Mater. 50 (2002) 793–803.
[19] J. Khalil-Allafi, A. Dlouhy, G. Eggeler, Ni_4Ti_3-precipitation during aging of NiTi shape memory alloys and its influence on martensitic phase transformations, Acta Mater. 50 (2002) 4255–4274.
[20] A. Dlouhy, J. Khalil-Allafi, G. Eggeler, Multiple-step martensitic transformations in Ni-rich NiTi alloys–an in-situ transmission electron microscopy investigation, Philos. Mag. 83 (2003) 339–363.
[21] M. Nishida, T. Hara, T. Ohba, K. Yamaguchi, K. Tanaka, K. Yamauchi, Experimental consideration of multistage martensitic transformation and precipitation behavior in aged Ni-rich Ti-Ni shape memory alloys, Mater. Trans. 44 (2003) 2631–2636.
[22] D. Stroz, D. Chrobak, Effect of internal strain on martensitic transformations in NiTi shape memory alloys, Mater. Trans. 52 (2011) 358–363.
[23] L. Bataillard, R. Gotthardt, Influence of thermal treatment on the appearance of a three step martensitic transformation in NiTi, J. Phys. IV 05 (1995) C8-647–C8-652.
[24] J. Michutta, C. Somsen, A. Yawny, A. Dlouhy, G. Eggeler, Elementary martensitic transformation processes in Ni-rich NiTi single crystals with Ni_4Ti_3 precipitates, Acta Mater. 54 (2006) 3525–3542.
[25] G. Fan, W. Chen, S. Yang, J. Zhu, X. Ren, K. Otsuka, Origin of abnormal multi--stage martensitic transformation behavior in aged Ni-rich Ti-Ni shape memory alloys, Acta Mater. 52 (2004) 4351–4362.
[26] J.I. Kim, Y. Liu, S. Miyazaki, Ageing-induced two-stage R-phase transformation in Ti–50.9at.%Ni, Acta Mater. 52 (2004) 487–499.
[27] Y. Wang, A.G. Khachaturyan, Three-dimensional field model and computer modeling of martensitic transformations, Acta Mater. 45 (1997) 759–773.
[28] J. Zhu, H. Wu, D. Wang, Y. Gao, H. Wang, Y. Hao, R. Yang, T.-Y. Zhang, Y. Wang, Crystallographic analysis and phase field simulation of transformation plasticity in a multifunctional β-Ti alloy, Int. J. Plast. 89 (2017) 110–129.
[29] W. Guo, I. Steinbach, C. Somsen, G. Eggeler, On the effect of superimposed external stresses on the nucleation and growth of Ni4Ti3 particles: A parametric phase field study, Acta Mater. 59 (2011) 3287–3296.
[30] N. Zhou, C. Shen, M.F.-X. Wagner, G. Eggeler, M.J. Mills, Y. Wang, Effect of Ni_4Ti_3 precipitation on martensitic transformation in Ti–Ni, Acta Mater. 58 (2010) 6685–6694.

[31] T.W. Yu, Y.P. Gao, L. Casalena, P.M. Anderson, M.J. Mills, Y. Wang, H-phase precipitation and its effect on martensitic transformation in NiTi-Hf high-temperature shape memory alloys, Acta Mater. (2021).
[32] Y. Wang, J. Li, Phase field modeling of defects and deformation, Acta Mater. 58 (2010) 1212–1235.
[33] L.-Q. Chen, Phase-field models for microstructure evolution, Annu. Rev. Mater. Res. 32 (2002) 113–140.
[34] D.Y. Li, L.Q. Chen, Shape of a rhombohedral coherent $Ti_{11}Ni_{14}$ precipitate in a cubic matrix and its growth and dissolution during constrained aging, Acta Mater. 45 (1997) 2435–2442.
[35] J. Wang, Y. Li, L.Q. Chen, T.Y. Zhang, The effect of mechanical strains on the ferroelectric and dielectric properties of a model single crystal–phase field simulation, Acta Mater. 53 (2005) 2495–2507.
[36] J. Wang, T.Y. Zhang, Phase field simulations of polarization switching-induced toughening in ferroelectric ceramics, Acta Mater. 55 (2007) 2465–2477.
[37] L.D. Landau, E.M. Lifshitz, Statistical Physics, Pergamon Press, Oxford, 1980.
[38] J.W. Cahn, J.E. Hilliard, Free energy of a nonuniform system. I. Interfacial free energy, J. Chem. Phys. 28 (1958) 258.
[39] J.W. Cahn, Free energy of a nonuniform system. II. Thermodynamic basis, J. Chem. Phys. 30 (1959) 1121–1124.
[40] A.G. Khachaturyan, Theory of Structural Transformations in Solids, John Wiley & Sons, New York, 1983.
[41] W. Tang, B. Sundman, R. Sandström, C. Qiu, New modelling of the B2 phase and its associated martensitic transformation in the Ti-Ni system, Acta Mater. 47 (1999) 3457–3468.
[42] N. Saunders, Cost 507: Thermochemical Database for Light Metal Alloys, Office for Official Publications of the European Communities, Luxembourg, 1998.
[43] E. Povoden-Karadeniz, D.C. Cirstea, P. Lang, T. Wojcik, E. Kozeschnik, Thermodynamics of Ti-Ni shape memory alloys, Calphad 41 (2013) 128–139.
[44] M. Nishida, C.M. Wayman, R. Kainuma, T. Honma, Further electron microscopy studies of the Ti_{11} Ni_{14} phase in an aged Ti52at%Ni shape memory alloy, Scr. Metall. 20 (1986) 899–904.
[45] V.I. Levitas, A.M. Roy, Multiphase phase field theory for temperature- and stress-induced phase transformations, Phys. Rev. B 91 (2015) 174109.
[46] J. Zhu, T. Zhang, Y. Yang, C.T. Liu, Phase field study of the copper precipitation in Fe-Cu alloy, Acta Mater. 166 (2019) 560–571.
[47] N. Hatcher, O.Y. Kontsevoi, A.J. Freeman, Role of elastic and shear stabilities in the martensitic transformation path of NiTi, Phys. Rev. B 80 (2009) 144203.
[48] J. Cahn, On spinodal decomposition, Acta Metall. 9 (1961) 795–801.
[49] J.D. Gunton, M.S. Miguel, P.S. Sahni, The dynamics of first order phase transitions, in: C. Domb, J. Lebowitz (Eds.), Phase Transitions Crit. Phenom., Academic Press, London, 1983, pp. 269–466.
[50] S.V. Divinski, I. Stloukal, L. Kral, C. Herzig, Diffusion of titanium and nickel in B2 NiTi, Defect Diffus. Forum. 289–292 (2009) 377–382.
[51] S. Miyazaki, C.M. Wayman, The R-phase transition and associated shape memory mechanism in Ti-Ni single crystals, Acta Metall. 36 (1988) 181–192.
[52] S.D. Prokoshkin, A.V. Korotitskiy, V. Brailovski, S. Turenne, I.Y. Khmelevskaya, I.B. Trubitsyna, On the lattice parameters of phases in binary Ti-Ni shape memory alloys, Acta Mater. 52 (2004) 4479–4492.
[53] D. Wang, S. Hou, Y. Wang, X. Ding, S. Ren, X. Ren, Y. Wang, Superelasticity of slim hysteresis over a wide temperature range by nanodomains of martensite, Acta Mater. 66 (2014) 349–359.
[54] E.M. Lifshitz, L.P. Pitaevskii, Statistical physics, part I, in: L.D. Landau, E.M. Lifshitz (Eds.), Course Theor. Phys., Pergamon Press, Oxford, 1980.
[55] Y.A. Izyumov, V.N. Syromyatnikov, Phase Transitions and Crystal Symmetry, Kluwer Academic Publishers, Boston, 1990.
[56] P. Tolédano, V. Dmitriev, Reconstructive Phase Transitions, World Scientific, New Jersey, 1996.
[57] Y. Wang, A.G. Khachaturyan, Multi-scale phase field approach to martensitic transformations, Mater. Sci. Eng. A 438–440 (2006) 55–63.
[58] M. Javanbakht, M.S. Ghaedi, E. Barchiesi, A. Ciallella, The effect of a pre-existing nanovoid on martensite formation and interface propagation: a phase field study, Math. Mech. Solids 26 (2021) 90–109.
[59] M. Javanbakht, M.S. Ghaedi, Nanovoid induced multivariant martensitic growth under negative pressure: effect of misfit strain and temperature on PT threshold stress and phase evolution, Mech. Mater. 151 (2020) 103627.
[60] M. Javanbakht, M. Sadegh Ghaedi, Thermal induced nanovoid evolution in the vicinity of an immobile austenite-martensite interface, Comput. Mater. Sci. 172 (2020) 109339.
[61] J. Khalil-Allafi, W.W. Schmahl, T. Reinecke, Order parameter evolution and Landau free energy coefficients for the B2↔ R-phase transition in a NiTi shape memory alloy, Smart Mater. Struct. 14 (2005) S192.
[62] A. Gyobu, Y. Kawamura, H. Horikawa, T. Saburi, Martensitic transformations in sputter-deposited shape memory Ti-Ni films, Mater. Trans. JIM 37 (1996) 697–702.
[63] J. Frenzel, A. Wieczorek, I. Opahle, B. Maaß, R. Drautz, G. Eggeler, On the effect of alloy composition on martensite start temperatures and latent heats in Ni–Ti-based shape memory alloys, Acta Mater. 90 (2015) 213–231.
[64] Z. Yang, W. Tirry, D. Schryvers, Analytical TEM investigations on concentration gradients surrounding Ni_4Ti_3 precipitates in Ni-Ti shape memory material, Scr. Mater. 52 (2005) 1129–1134.
[65] B. Karbakhsh Ravari, S. Farjami, M. Nishida, Effects of Ni concentration and aging conditions on multistage martensitic transformation in aged Ni-rich Ti–Ni alloys, Acta Mater. 69 (2014) 17–29.
[66] Y. Ji, X. Ding, T. Lookman, K. Otsuka, X. Ren, Heterogeneities and strain glass behavior: role of nanoscale precipitates in low-temperature-aged $Ti_{48.7}Ni_{51.3}$ alloys, Phys. Rev. B 87 (2013) 104110.
[67] C.-É. Guillaume, Recherches sur les aciers au nickel, J. Phys. Théor. Appl. 7 (1898) 262–274.
[68] Y. Wang, J. Gao, H. Wu, S. Yang, X. Ding, D. Wang, X. Ren, Y. Wang, X. Song, J. Gao, Strain glass transition in a multifunctional β-type Ti alloy, Sci. Rep. 4 (2014) 3995.
[69] L. Zhang, D. Wang, X. Ren, Y. Wang, A new mechanism for low and temperature-independent elastic modulus, Sci. Rep. 5 (2015) 11477.
[70] J. Uchil, K.P. Mohanchandra, K. Ganesh Kumara, K.K. Mahesh, T.P. Murali, Thermal expansion in various phases of Nitinol using TMA, Phys. B Condens. Matter 270 (1999) 289–297.
[71] A.T. Dinsdale, SGTE data for pure elements, 15 (1991) 317–425.
[72] G.B. Stachowiak, P.G. McCormick, Shape memory behaviour associated with the R and martensitic transformations in a NiTi alloy, Acta Metall 36 (1988) 291–297.